Cas9 dynamics in living cells and offer insight into how Cas9 navigates hierarchical organization of DNA within a eukaryotic nucleus.

REFERENCES AND NOTES

1. M. Jinek *et al.*, *Science* **337**, 816–821 (2012).
2. G. Gasiunas, R. Barrangou, P. Horvath, V. Siksnys, *Proc. Natl. Acad. Sci. U.S.A.* **109**, E2579–E2586 (2012).
3. P. D. Hsu, E. S. Lander, F. Zhang, *Cell* **157**, 1262–1278 (2014).
4. J. A. Doudna, E. Charpentier, *Science* **346**, 1258096 (2014).
5. R. M. Terns, M. P. Terns, *Trends Genet.* **30**, 111–118 (2014).
6. S. H. Sternberg, S. Redding, M. Jinek, E. C. Greene, J. A. Doudna, *Nature* **507**, 62–67 (2014).
7. M. Jinek *et al.*, *Science* **343**, 1247997 (2014).
8. H. Nishimasu *et al.*, *Cell* **156**, 935–949 (2014).
9. C. Anders, O. Niewoehner, A. Duerst, M. Jinek, *Nature* **513**, 569–573 (2014).
10. X. Wu *et al.*, *Nat. Biotechnol.* **32**, 670–676 (2014).
11. C. Kuscu, S. Arslan, R. Singh, J. Thorpe, M. Adli, *Nat. Biotechnol.* **32**, 677–683 (2014).
12. P. D. Hsu *et al.*, *Nat. Biotechnol.* **31**, 827–832 (2013).
13. V. Pattanayak *et al.*, *Nat. Biotechnol.* **31**, 839–843 (2013).
14. B. Chen *et al.*, *Cell* **155**, 1479–1491 (2013).
15. G. V. Los *et al.*, *ACS Chem. Biol.* **3**, 373–382 (2008).
16. J. B. Grimm *et al.*, *Nat. Methods* **12**, 244–250, 3, 250 (2015).
17. J. Jurka, O. Kohany, A. Pavlicek, V. V. Kapitonov, M. V. Jurka, *Cytogenet. Genome Res.* **110**, 117–123 (2005).
18. C. A. Espinoza, J. A. Goodrich, J. F. Kugel, *RNA* **13**, 583–596 (2007).
19. S. Abrahamsson *et al.*, *Nat. Methods* **10**, 60–63 (2013).
20. J. C. M. Gebhardt *et al.*, *Nat. Methods* **10**, 421–426 (2013).
21. D. Normanno *et al.*, *Nat. Commun.* **6**, 7357 (2015).
22. M. D. Szczelkun *et al.*, *Proc. Natl. Acad. Sci. U.S.A.* **111**, 9798–9803 (2014).
23. B. L. Sprague, R. L. Pego, D. A. Stavreva, J. G. McNally, *Biophys. J.* **86**, 3473–3495 (2004).
24. F. Mueller, D. Mazza, T. J. Stasevich, J. G. McNally, *Curr. Opin. Cell Biol.* **22**, 403–411 (2010).
25. J. C. Eissenberg, S. C. R. Elgin, *Curr. Opin. Genet. Dev.* **10**, 204–210 (2000).
26. Z. Liu *et al.*, *eLife* **3**, e04236 (2014).
27. S. Manley *et al.*, *Nat. Methods* **5**, 155–157 (2008).
28. Materials and Methods are available as supplementary materials on *Science* Online.
29. M. El Beheiry, M. Dahan, J. B. Masson, *Nat. Methods* **12**, 594–595 (2015).
30. I. Izeddin *et al.*, *eLife* **3**, e02230 (2014).

ACKNOWLEDGMENTS

We thank L. Lavis for generously providing HaloTag ligands for imaging experiments; J. Macklin for expert assistance with FCS experiments; and X. Darzacq, R. Singer, J. Cate, and members of the Doudna and Tjian labs for helpful discussions and critical reading of the manuscript. S.C.K. acknowledges support from the Janelia Visitor Program, S.C.K. and E.T.Z. acknowledge support from the National Science Foundation Graduate Research Fellowship Program, W.D. acknowledges support from the Helen Hay Whitney Foundation, and Z.L. acknowledges support from the Janelia Fellow Program. Funding was provided by the National Science Foundation (MCB-1244557 to J.A.D.) and the California Institute for Regenerative Medicine (CIRM, RB4-06016 to R.T.). J.A.D. and R.T. are Investigators of the Howard Hughes Medical Institute. This work was performed in part at the University of California Berkeley Cancer Research Laboratory Molecular Imaging Center, supported by the Gordon and Betty Moore Foundation. J.A.D. is a co-founder of Caribou Biosciences, Inc., Editas Medicine and Intellia Therapeutics.

SUPPLEMENTARY MATERIALS

www.sciencemag.org/content/350/6262/823/suppl/DC1
Materials and Methods
Table S1
Figs. S1 to S13
Captions for Movies S1 to S12
References (*31*–*38*)
Movies S1 to S12

27 May 2015; accepted 7 October 2015
10.1126/science.aac6572

ANTIVIRAL IMMUNITY

Nlrp6 regulates intestinal antiviral innate immunity

Penghua Wang,[1,6]* Shu Zhu,[2]* Long Yang,[1,6] Shuang Cui,[1] Wen Pan,[3] Ruaidhri Jackson,[2] Yunjiang Zheng,[2] Anthony Rongvaux,[2] Qiangming Sun,[1]† Guang Yang,[1]‡ Shandian Gao,[1] Rongtuan Lin,[4] Fuping You,[1] Richard Flavell,[2,5]§|| Erol Fikrig[1,5]§||

The nucleotide-binding oligomerization domain–like receptor (Nlrp) 6 maintains gut microbiota homeostasis and regulates antibacterial immunity. We now report a role for Nlrp6 in the control of enteric virus infection. *Nlrp6*$^{-/-}$ and control mice systemically challenged with encephalomyocarditis virus had similar mortality; however, the gastrointestinal tract of *Nlrp6*$^{-/-}$ mice exhibited increased viral loads. *Nlrp6*$^{-/-}$ mice orally infected with encephalomyocarditis virus had increased mortality and viremia compared with controls. Similar results were observed with murine norovirus 1. Nlrp6 bound viral RNA via the RNA helicase Dhx15 and interacted with mitochondrial antiviral signaling protein to induce type I/III interferons (IFNs) and IFN-stimulated genes (ISGs). These data demonstrate that Nlrp6 functions with Dhx15 as a viral RNA sensor to induce ISGs, and this effect is especially important in the intestinal tract.

Nucleotide oligomerization domain (NOD)–like receptors (NLRs) play a central role in the immune response to diverse microorganisms and react to environmental insults and cellular danger signals (*1*, *2*). Some NLRs contribute to antiviral immunity. NOD2 recognizes single-stranded RNA (ssRNA) viruses to induce type I interferons (IFNs) via mitochondrial antiviral-signaling protein (MAVS) (*3*), and the NLRP3 inflammasome is crucial for the control of diverse viral infections in vivo (*4*–*7*). Several NLRs, on the other hand, dampen antiviral immune responses. NLRX1 and NLRC5 negatively regulate type I IFNs and nuclear factor κB (NF-κB) signaling via distinct molecular mechanisms (*8*–*12*); NLRC3 attenuates Toll-like receptor signaling and the stimulator of interferon genes (STING)–mediated anti-DNA virus immune signaling (*13*, *14*). A role for Nlrp6 in the regulation of antibacterial immune responses has recently been documented (*15*–*18*); however, whether Nlrp6 regulates viral infection has not yet been elucidated.

Nlrp6 exhibits a tissue- and cell-type–specific pattern of expression, with the highest level in intestinal epithelial cells (IECs) (*15*) (figs. S1 and S2). We therefore determined whether Nlrp6 plays a prominent role in inhibiting enteric virus infection at the intestinal interface. We used a (+) ssRNA virus, encephalomyocarditis virus (EMCV), which is transmitted via the fecal-oral route in nature. We infected both wild-type (WT) and *Nlrp6*$^{-/-}$ mice with EMCV systemically via intraperitoneal injection and noted that the survival curve of *Nlrp6*$^{-/-}$ mice was similar to that of WT animals (Fig. 1A). Viral dissemination was also the same in the blood, brains, and hearts of *Nlrp6*$^{-/-}$ and WT mice. The intestinal viral burden of *Nlrp6*$^{-/-}$ mice was, however, higher than that of WT animals (Fig. 1B)—suggesting that Nlrp6 plays an important role in limiting EMCV replication at this location. In support of this, *Nlrp6* mRNA expression was much higher in the intestines than other tissues after EMCV infection (Fig. 1C). We therefore reasoned that Nlrp6 prevents systemic infection and mortality when EMCV is delivered orally to its principal site of infection—the intestine. Indeed, *Nlrp6*$^{-/-}$ mice were more susceptible to oral infection with EMCV than WT animals (Fig. 1D and Fig. 3E).

Alterations in microbiota and inflammasome activation are two potential processes that may influence the ability of *Nlrp6*$^{-/-}$ mice to control intestinal EMCV infection. The intestinal microbial ecology of *Nlrp6*$^{-/-}$ mice is different from that of WT mice (*15*), which could affect antiviral immunity. We therefore cohoused mice for 4 weeks before EMCV infection, which we previously showed was sufficient to equilibrate the microbiota between WT and *Nlrp6*$^{-/-}$ mice. WT and *Nlrp6*$^{-/-}$ mice had similar levels of *TM7* and *Prevotellacae* bacteria (*15*) after cohousing (fig. S3A), indicating stabilization of the microbiota. *Nlrp6*$^{-/-}$ mice, however, died of EMCV infection more rapidly than WT and cohoused WT animals (Fig. 1D), and viremia was ~10-fold higher in *Nlrp6*$^{-/-}$ than WT animals (Fig. 1E). When inoculated systemically

[1]Section of Infectious Diseases, Yale University School of Medicine, 300 Cedar Street, New Haven, CT 06510, USA. [2]Department of Immunobiology, Yale University School of Medicine, 300 Cedar Street, New Haven, CT 06510, USA. [3]Department of Genetics, Yale University School of Medicine, 300 Cedar Street, New Haven, CT 06510, USA. [4]Lady Davis Institute, Department of Medicine, McGill University, Montreal, Quebec, Canada. [5]Howard Hughes Medical Institute, Chevy Chase, MD 20815-6789, USA. [6]Department of Microbiology and Immunology, New York Medical College, Valhalla, NY 10595, USA.
*These authors contributed equally to this work. †Present address: Institute of Medical Biology, Chinese Academy of Medical Sciences, and Peking Union Medical College, Kunming, People's Republic of China. ‡Present address: Department of Parasitology, School of Medicine, Jinan University, Guangzhou, China. §The laboratories of these authors contributed equally to this work. **||Corresponding author. E-mail: richard.flavell@yale.edu (R.F.); erol.fikrig@yale.edu (E.F.)**

via intraperitoneal injection, EMCV loads in the intestines of cohoused *Nlrp6*$^{-/-}$ mice were also more than 10-fold higher than those of cohoused WT animals (Fig. 1F). Similar survival results were noted for *Nlrp6*$^{-/-}$ and *Nlrp6*$^{+/+}$ littermates (fig. S3B). These data demonstrate that the increased viral susceptibility of *Nlrp6*$^{-/-}$ mice is not a result of altered intestinal microbial ecology. To extend our finding further, we examined another enteric virus, murine norovirus 1 (MNV-1), a (+) ssRNA virus. MNV-1 was rapidly cleared by the innate immune system in WT mice (*19*) but persisted much longer in *Nlrp6*$^{-/-}$ mice (fig. S3, C to E). Nlrp6 initiates inflammasome signaling via caspase-1. We therefore determined whether Nlrp6 requires caspase-1 to control EMCV at the intestinal epithelia. In agreement with a previous report (*20*), following EMCV challenge, the survival of *Casp1*$^{-/-}$ and WT mice was similar (Fig. 1D). These data suggest that intestinal Nlrp6 controls EMCV infection by an alternative mechanism.

To understand how Nlrp6 contributes to antiviral innate immune responses, we used an Nlrp6 antibody to immunoprecipitate Nlrp6 binding partners from mouse primary IECs and a FLAG-Nlrp6 overexpression system in human embryonic kidney 293 T (HEK293T) cells. We identified DEAH (Asp-Glu-Ala-His) box helicase 15 (Dhx15) by mass spectrometry (fig. S4) and confirmed it using a specific antibody to Dhx15 (Fig. 2A and fig. S5A). Glutathione *S*-transferase–Dhx15 expressed in *Escherichia coli* pulled down FLAG-Nlrp6 expressed using a mammalian in vitro translation system (fig. S5B), suggesting a direct interaction. Nlrp6 is composed of three functional domains: an N-terminal pyrin domain (PYD), a NACHT domain, and a C-terminal leucine-rich repeat domain (LRR). Each individual domain failed to bind Dhx15 when compared with full-length Nlrp6 (fig. S5C). A fragment encompassing the NATCH and NACHT-associated domain (NAD) interacted with Dhx15 (Fig. 2B). NLRP3, a close relative of Nlrp6, did not interact with Dhx15, demonstrating specificity (fig. S5C).

Dhx15 is a putative pre-mRNA-splicing factor and adenosine triphosphate (ATP)–dependent RNA helicase that modulates antiviral immune responses via MAVS, an adaptor protein for retinoic acid inducible gene 1 (RIG-I)–like receptors (RLRs) (*21*, *22*). We reasoned that the Nlrp6-Dhx15 complex might use MAVS to trigger type I IFN responses. Indeed, FLAG-Nlrp6 bound endogenous MAVS, as did Nlrp3 ((*23*)) and RIG-I (*24*–*27*) (Fig. 2C). The negative controls FLAG-NLRC5 (*11*) or Nlrp10 did not coprecipitate with MAVS (fig. S5D), confirming the specificity of the Nlrp6-MAVS interaction. Because Dhx15 is a putative RNA helicase and viral RNA sensor (*22*), we then determined whether Nlrp6-Dhx15 forms a viral RNA-sensing complex. Both Nlrp6 and Dhx15 showed high affinity for viral RNA (Fig. 2D and fig. S6A). The Nlrp6 NACHT domain was sufficient for RNA binding but weaker than full-length Nlrp6 (fig. S6B). To exclude nonspecific binding due to overexpression, we examined endogenous Nlrp6 binding to viral RNA in WT and FLAG-Nlrp6 knock-in mice (fig. S2). Both Nlrp6 and FLAG-Nlrp6 was coimmunoprecipitated with EMCV RNA from infected IECs (Fig. 2E and fig. S6C). Because the RNA binding capacity of Dhx15 was much greater than that of Nlrp6, we reasoned that Nlrp6-RNA binding was dependent on Dhx15. Indeed, the amount of Nlrp6-bound viral RNA was reduced significantly in Dhx15 small interfering RNA (siRNA)–treated cells (Fig. 2F). In contrast, Dhx15-RNA binding was not altered in *Nlrp6*$^{-/-}$ cells (fig. S6D). Like Dhx15 (*22*), Nlrp6 bound only RNA but not DNA viruses (fig. S6E). To assess the nature of viral RNA bound by Nlrp6, we tested several synthetic RNA analogs. Nlrp6 preferably bound the long double-stranded RNA (dsRNA) analog polyinosinic-polycytidylic acid (polyIC) (Fig. 2G). To provide in vivo evidence for a functional interaction between MAVS, Dhx15, and Nlrp6, we examined MAVS-Dhx15 interactions in WT and *Nlrp6*$^{-/-}$IECs. Consistent with a previous report (*22*), MAVS binding to Dhx15 was enhanced by EMCV infection in WT IECs, but the interaction was weaker in *Nlrp6*$^{-/-}$ (Fig. 2H). *Mavs*$^{-/-}$ mice

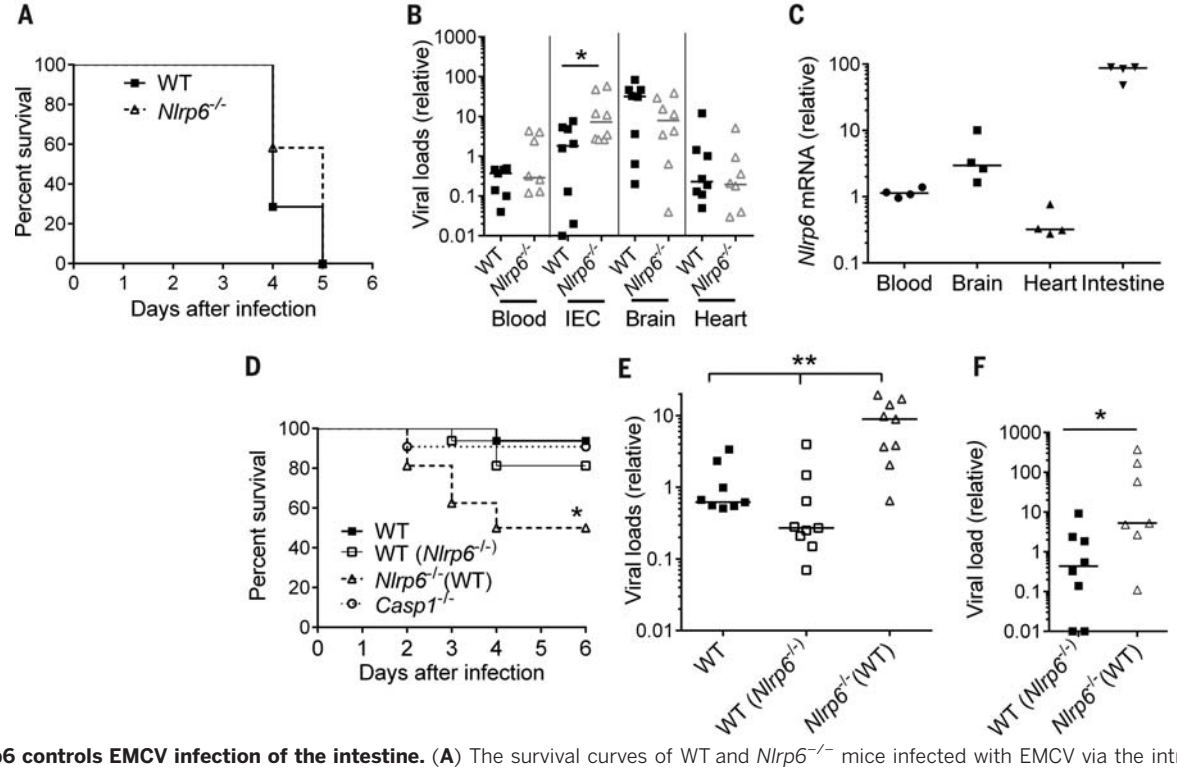

Fig. 1. Nlrp6 controls EMCV infection of the intestine. (**A**) The survival curves of WT and *Nlrp6*$^{-/-}$ mice infected with EMCV via the intraperitoneal route. *N* = 12 mice per group. (**B** and **C**) Quantitative polymerase chain reaction (qPCR) analyses of (B) EMCV viral loads and (C) *Nlrp6* in various tissues 72 hours after infection with EMCV intraperitoneally Intestinal epithelial cells (IEC). (**D**) The survival curves of WT mice, WT mice cohoused with *Nlrp6*$^{-/-}$ [WT (*Nlrp6*$^{-/-}$)], *Nlrp6*$^{-/-}$ mice cohoused with WT [*Nlrp6*$^{-/-}$(WT)], and *Casp1*$^{-/-}$ mice after oral infection with EMCV. *N* = 10 to 16 mice per group. *P < 0.05 (log-rank test). Results were pooled from two independent experiments. (**E** and **F**) qPCR analysis of EMCV loads (E) in the whole blood cells 72 hours after oral infection or (F) in the intestines 72 hours after intraperitoneal infection. Each symbol in (B), (C), (E), and (F) represents one mouse; small horizontal lines indicate the median of the result. *P < 0.05; **P < 0.01 (nonparametric Mann-Whitney analysis). The data are representative of at least two to three independent experiments.

were also much more susceptible to EMCV administered orally when compared with WT mice (Fig. 2I). These data suggest that the Dhx15-Nlrp6-MAVS axis plays an important role in restricting EMCV infection of the intestine.

To validate a role for Nlrp6 in Dhx15-Mavs–mediated antiviral immunity, we examined the expression of type I/III IFN-induced genes (ISGs). The mRNA and protein expression of a number of ISGs was reduced in *Nlrp6*$^{-/-}$ IECs compared with WT (fig. S7A and Fig. 3, A and B). Although both types I and III IFNs can elicit antiviral responses, type III IFNs are particularly critical for controlling viral infection in IECs (*28*–*30*). IFN-λ (also known as IL-28a) protein and mRNA, and *Ifnb* mRNA, were reduced in *Nlrp6*$^{-/-}$ intestines after EMCV infection (fig. S7B). ISG mRNA amounts were, however, similar in other WT and *Nlrp6*$^{-/-}$ tissues (fig. S8).

To assess whether the Nlrp6-caspase-1 inflammasome regulates antiviral immunity in the intestine, we compared ISG expression in *Nlrp6*$^{-/-}$ with *Casp1*$^{-/-}$ and WT mice. The viral loads and ISG expression were similar in the intestines of *Casp1*$^{-/-}$ and WT mice (fig. S9), demonstrating an inflammasome-independent antiviral mechanism for Nlrp6. In support of the in vivo findings, EMCV loads in *Nlrp6*$^{-/-}$ embryonic fibroblasts (MEFs) were sixfold higher than those in *Nlrp6*$^{+/-}$ cells at 16 hours after infection, while antiviral gene expression was significantly lower (Fig. 3, C and D, and fig. S10, A and B). We also observed a decrease in polyIC-induced *Ifnb1* expression in *Nlrp6*$^{-/-}$ compared with *Nlrp6*$^{-/+}$ MEFs (fig. S10C). In agreement with the results from *Nlrp6*$^{-/-}$ cells, overexpression of Nlrp6 enhanced *Ifnb1* and *Il6* expression modestly (fig. S11). All these data demonstrate a pivotal role for Nlrp6 in inducing type I/III IFNs and ISGs. Type III IFNs are particularly critical for control of viral infection of IECs (*28*–*30*). Indeed, exogenous IFN-λ fully protected WT and *Nlrp6*$^{-/-}$ mice against lethal EMCV infection and reduced viremia significantly (Fig. 3E). We next determined whether the antiviral function of Nlrp6 is specific for RNA viruses. Neither herpes simplex virus–1 (HSV-1) titers nor *Ifnb1* expression in *Nlrp6*$^{-/-}$ was different from those in *Nlrp6*$^{-/+}$ cells (fig. S12A). IFN-α, polydAT, or lipopolysaccharide-induced ISGs or cytokine expression in *Nlrp6*$^{-/-}$ was also similar to that in *Nlrp6*$^{-/+}$ MEFs (fig. S12, B to D).

As viral infections and the ligands that can induce robust type I IFN expression also upregulated Nlrp6 expression (Fig. 3C and figs. S10C, S12C, and S13), we reasoned that Nlrp6 per se might be an ISG. Indeed, induction of *Nlrp6* mRNA expression by EMCV or polyIC

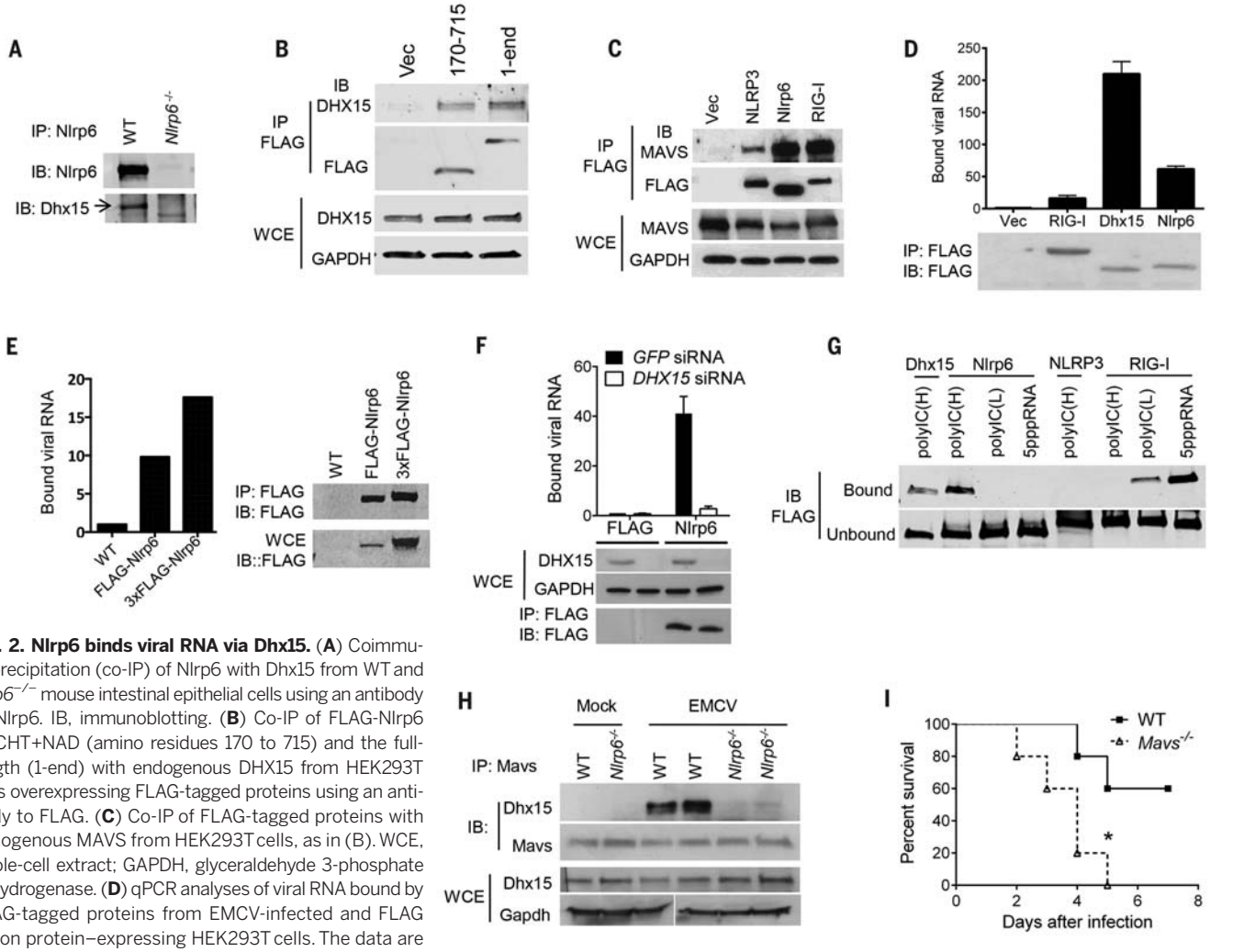

Fig. 2. Nlrp6 binds viral RNA via Dhx15. (**A**) Coimmunoprecipitation (co-IP) of Nlrp6 with Dhx15 from WT and *Nlrp6*$^{-/-}$ mouse intestinal epithelial cells using an antibody to Nlrp6. IB, immunoblotting. (**B**) Co-IP of FLAG-Nlrp6 NACHT+NAD (amino residues 170 to 715) and the full-length (1-end) with endogenous DHX15 from HEK293T cells overexpressing FLAG-tagged proteins using an antibody to FLAG. (**C**) Co-IP of FLAG-tagged proteins with endogenous MAVS from HEK293T cells, as in (B). WCE, whole-cell extract; GAPDH, glyceraldehyde 3-phosphate dehydrogenase. (**D**) qPCR analyses of viral RNA bound by FLAG-tagged proteins from EMCV-infected and FLAG fusion protein–expressing HEK293T cells. The data are presented as relative increase over vector (FLAG). (**E**) Binding of endogenous Nlrp6 to viral RNA. (Left) qPCR analyses of viral RNA bound by endogenous FLAG-Nlrp6 in IECs. (Right) Immunoblots of FLAG-Nlrp6 in WCE and IP. 3xFLAG-Nlrp6 denotes three FLAG motifs tagged to Nlrp6. (**F**) (Top) qPCR analyses of EMCV RNA bound by FLAG-Nlrp6 from *GFP* or *DHX15* siRNA-treated HEK293T cells. (Bottom) Immunoblots of WCE and IP. (**G**) Immunoblots showing FLAG-tagged proteins (purified from HEK293T) bound by biotin-labeled RNA analogs. polyIC(H), high molecular weight (1.5 to 8 kb); polyIC(L), low molecular weight (0.2 to 1 kb). (**H**) Co-IP of Mavs with Dhx15 from IECs of WT and *Nlrp6*$^{-/-}$ mice infected with EMCV using a rabbit polyclonal antibody to Mavs. (**I**) The survival curves of WT and *Mavs*$^{-/-}$ mice after oral infection with EMCV. $N = 5$ mice per group; $^*P < 0.05$ (log-rank test). The data are representative of at least two independent experiments.

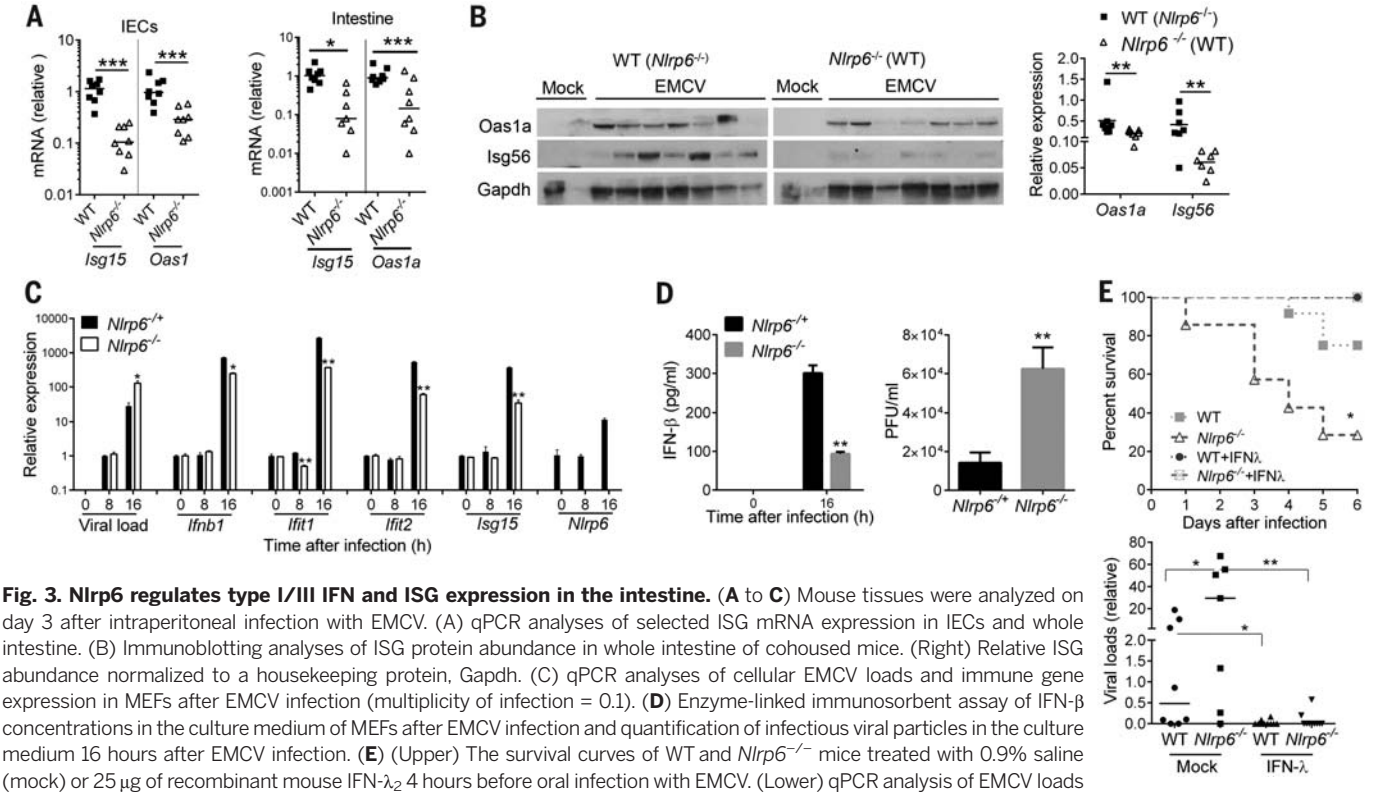

Fig. 3. Nlrp6 regulates type I/III IFN and ISG expression in the intestine. (**A** to **C**) Mouse tissues were analyzed on day 3 after intraperitoneal infection with EMCV. (A) qPCR analyses of selected ISG mRNA expression in IECs and whole intestine. (B) Immunoblotting analyses of ISG protein abundance in whole intestine of cohoused mice. (Right) Relative ISG abundance normalized to a housekeeping protein, Gapdh. (C) qPCR analyses of cellular EMCV loads and immune gene expression in MEFs after EMCV infection (multiplicity of infection = 0.1). (**D**) Enzyme-linked immunosorbent assay of IFN-β concentrations in the culture medium of MEFs after EMCV infection and quantification of infectious viral particles in the culture medium 16 hours after EMCV infection. (**E**) (Upper) The survival curves of WT and *Nlrp6*$^{-/-}$ mice treated with 0.9% saline (mock) or 25 μg of recombinant mouse IFN-λ_2 4 hours before oral infection with EMCV. (Lower) qPCR analysis of EMCV loads in the whole blood cells 72 hours after infection. $N = 7$ to 10 mice per group. *$P < 0.05$ (log-rank test). In (A) and (E), the data are normalized with mouse beta actin and are presented as relative change over the mean of the results of WT [Mock-WT in (E)] mice. Each band/dot represents an animal. The horizontal lines in the figures indicate the median of the results. *$P < 0.05$; **$P < 0.01$; ***$P < 0.001$ (nonparametric Mann-Whitney analysis). In (C) and (D), scale bars show mean + SEM; $n = 3$ mice. *$P < 0.05$; **$P < 0.01$ (unpaired Students' t test). The data are representative of at least two independent experiments.

Fig. 4. Nlrp6 is an ISG. qPCR analyses of the transcripts of (**A**) *Nlrp6* and (**B**) *Mda5* in WT, *Irf3/7*$^{-/-}$, and *Ifnar*$^{-/-}$ MEFs treated with EMCV, polyIC, recombinant IFN-α, or TNF-α. The data are expressed as percentage of a housekeeping gene *Hprt*. Scale bars, mean + SD. The data are representative of at least two independent experiments.

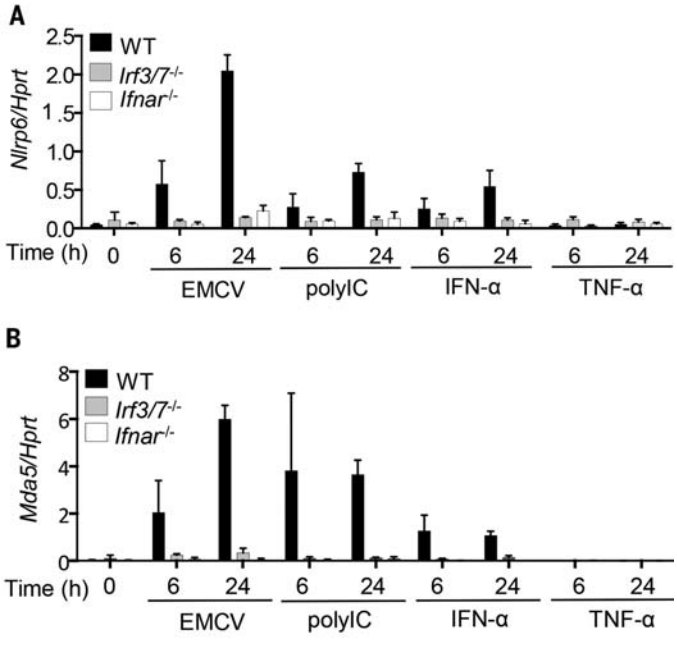

treatment was almost abolished in *Irf3/7*$^{-/-}$ or *Ifnar1*$^{-/-}$ MEFs. Consistent with this, recombinant IFN-α, but not tumor necrosis factor–α (TNF-α) was able to induce *Nlrp6* expression vigorously, suggesting that interferon regulatory factor (IRF)/IFN signaling, but not NF-κB signaling controls Nlrp6 expression (Fig. 4 and fig. S14A). *Nlrp6* mRNA expression was also induced by recombinant IFN-λ2 (fig. S14B). These results indicate that *Nlrp6* expression is regulated by type I/III IFNs via IRF3/7.

The above-mentioned data demonstrate that Dhx15-Nlrp6 senses long dsRNA in the cytoplasm (Fig. 2G), a well-established feature for MDA5. We then determined whether Nlrp6-mediated signaling is also dependent on MDA5. siRNA knockdown of Nlrp6 reduced *Ifnb1* and *Isg15* mRNA expression after polyIC stimulation in *Mda5*$^{-/-}$ MEFs (fig. S15A), suggesting an MDA5-independent antiviral role for Nlrp6. Similar results were noted with *Rig-I*$^{-/-}$ MEFs (fig. S15B). Nlrp6-RNA binding was unchanged in *Mda5*$^{-/-}$ or *Rig-I*$^{-/-}$ MEFs compared with WT (fig. S15C), and there was no interaction between Nlrp6 and MDA5 or RIG-I (fig. S15D). We next examined the relative antiviral role for MDA5 in the intestine in comparison with Nlrp6. The viral loads in both *Nrp6*$^{-/-}$ and *Mda5*$^{-/-}$ IECs were similar but were much higher than those in WT mice (fig. S15E). These results, in conjunction with the Nlrp6, Dhx15, and MDA5 expression data (fig. S1), suggest that Dhx15-Nlrp6 constitutes the first line of anti-EMCV defense in the intestinal epithelia, whereas MDA5 is dominant in myeloid cells.

Our results demonstrate that Nlrp6 controls enteric virus infection in the intestine by interacting with an RNA sensor, Dhx15, to trigger MAVS-dependent antiviral responses. This inflammasome-independent response provides a mechanism for Nlrp6 to elicit pleotropic effects in the host and demonstrates its importance against diverse classes of microbes.

REFERENCES AND NOTES

1. K. Schroder, J. Tschopp, *Cell* **140**, 821–832 (2010).
2. T. Strowig, J. Henao-Mejia, E. Elinav, R. Flavell, *Nature* **481**, 278–286 (2012).
3. A. Sabbah *et al.*, *Nat. Immunol.* **10**, 1073–1080 (2009).
4. T. Ichinohe, H. K. Lee, Y. Ogura, R. Flavell, A. Iwasaki, *J. Exp. Med.* **206**, 79–87 (2009).
5. I. C. Allen *et al.*, *Immunity* **30**, 556–565 (2009).
6. T. D. Kanneganti *et al.*, *Nature* **440**, 233–236 (2006).
7. P. G. Thomas *et al.*, *Immunity* **30**, 566–575 (2009).
8. C. B. Moore *et al.*, *Nature* **451**, 573–577 (2008).
9. I. C. Allen *et al.*, *Immunity* **34**, 854–865 (2011).
10. Y. Lei *et al.*, *Immunity* **36**, 933–946 (2012).
11. J. Cui *et al.*, *Cell* **141**, 483–496 (2010).
12. Y. Tong *et al.*, *Cell Res.* **22**, 822–835 (2012).
13. M. Schneider *et al.*, *Nat. Immunol.* **13**, 823–831 (2012).
14. L. Zhang *et al.*, *Immunity* **40**, 329–341 (2014).
15. E. Elinav *et al.*, *Cell* **145**, 745–757 (2011).
16. K. Kersse, M. J. Bertrand, M. Lamkanfi, P. Vandenabeele, *Cytokine Growth Factor Rev.* **22**, 257–276 (2011).
17. M. Wlodarska *et al.*, *Cell* **156**, 1045–1059 (2014).
18. P. K. Anand *et al.*, *Nature* **488**, 389–393 (2012).
19. S. M. Karst, C. E. Wobus, M. Lay, J. Davidson, H. W. Virgin 4th, *Science* **299**, 1575–1578 (2003).
20. J. V. Rajan, D. Rodriguez, E. A. Miao, A. Aderem, *J. Virol.* **85**, 4167–4172 (2011).
21. K. Mosallanejad *et al.*, *Sci. Signal.* **7**, ra40 (2014).
22. H. Lu *et al.*, *J. Immunol.* **193**, 1364–1372 (2014).
23. N. Subramanian, K. Natarajan, M. R. Clatworthy, Z. Wang, R. N. Germain, *Cell* **153**, 348–361 (2013).
24. T. Kawai *et al.*, *Nat. Immunol.* **6**, 981–988 (2005).
25. E. Meylan *et al.*, *Nature* **437**, 1167–1172 (2005).
26. R. B. Seth, L. Sun, C. K. Ea, Z. J. Chen, *Cell* **122**, 669–682 (2005).
27. L. G. Xu *et al.*, *Mol. Cell* **19**, 727–740 (2005).
28. J. Pott *et al.*, *Proc. Natl. Acad. Sci. U.S.A.* **108**, 7944–7949 (2011).
29. A. H. Broquet, Y. Hirata, C. S. McAllister, M. F. Kagnoff, *J. Immunol.* **186**, 1618–1626 (2011).
30. T. J. Nice *et al.*, *Science* **347**, 269–273 (2015).

ACKNOWLEDGMENTS

The data presented in this manuscript are tabulated in the main paper and in the supplementary materials. This work was supported by National Institutes of Health grants N01-HHSN272011000019C, AI099625, and AI103807. E.F. and R.F. are Investigators of the Howard Hughes Medical Institute. S.Z. was supported by a fellowship from Howard Hughes Medical Institute–The Helen Hay Whitney Foundation.

SUPPLEMENTARY MATERIALS

www.sciencemag.org/content/350/6262/826/suppl/DC1
Materials and Methods
Figs. S1 to S15
References (*31*–*37*)

9 April 2015; accepted 2 October 2015
Published online 22 October 2015
10.1126/science.aab3145

MUCOSAL IMMUNITY

A gut-vascular barrier controls the systemic dissemination of bacteria

Ilaria Spadoni,[1] Elena Zagato,[1] Alice Bertocchi,[1] Roberta Paolinelli,[2] Edina Hot,[1] Antonio Di Sabatino,[3] Flavio Caprioli,[4] Luca Bottiglieri,[5] Amanda Oldani,[2] Giuseppe Viale,[5] Giuseppe Penna,[1] Elisabetta Dejana,[2,6,7] Maria Rescigno[1,6]*

In healthy individuals, the intestinal microbiota cannot access the liver, spleen, or other peripheral tissues. Some pathogenic bacteria can reach these sites, however, and can induce a systemic immune response. How such compartmentalization is achieved is unknown. We identify a gut-vascular barrier (GVB) in mice and humans that controls the translocation of antigens into the bloodstream and prohibits entry of the microbiota. *Salmonella typhimurium* can penetrate the GVB in a manner dependent on its pathogenicity island (Spi) 2–encoded type III secretion system and on decreased β-catenin–dependent signaling in gut endothelial cells. The GVB is modified in celiac disease patients with elevated serum transaminases, which indicates that GVB dismantling may be responsible for liver damage in these patients. Understanding the GVB may provide new insights into the regulation of the gut-liver axis.

Upon ingestion, food antigens can access the lymphatics to reach the mesenteric lymph nodes (MLNs) (*1*) and the blood stream (portal vein) to reach the liver (*2*). In contrast, the microbiota cannot access the liver (*3*) and can reach the spleen only when the MLNs are excised (*4*). This suggests that the microbiota are actively excluded from the bloodstream and that the MLNs provide a firewall for the systemic dissemination of the microbiota from the lymphatics (*5*). What determines antigen access to the bloodstream is unknown.

We hypothesized the existence of a gut-vascular barrier (GVB) that might control the type of antigens that are translocated across blood endothelial cells (ECs) to reach the portal vein. To evaluate the presence of such a barrier, we injected mice intravenously with fluorescein isothiocyanate (FITC)–dextran of different molecular sizes and analyzed leakage of the dye into the intestine. We observed that there is an endothelial barrier that discriminates between differently sized particles of the same nature. FITC-dextran of 4 kD freely diffused through the ECs, whereas FITC-dextran of 70 kD could not (Fig. 1A; fig. S1, A and B; and movies S1 and S2). However, after oral infection with *Salmonella enterica* serovar Typhimurium, which disseminates systemically in mice (*6*), 70 kD dextran was readily released from the bloodstream (Fig. 1A, fig. S1, and movies S3 and S4). This was not due to increased blood flow during infection, as 1-μm microspheres were retained within the vessels even after *Salmonella* infection (fig. S1, C and D, and movies S5 and S6). These results suggest the existence of a GVB that prevents the translocation of molecules of around 70 kD and that can be disrupted by *Salmonella*.

Endothelial barriers are characterized by the presence of elaborate junctional complexes that include tight junction (TJ) and adherens junction (AJ), which strictly control paracellular trafficking of solutes and fluids (*7*, *8*). Other cell types, such as pericytes or fibroblasts, can be found associated with the microvasculature and are involved in the maintenance of the vascular barrier, where they form a vascular unit (*9*). To study GVB characteristics, we analyzed the composition of TJ and AJ in gut ECs. We found that enteric ECs have TJ formed by occludin, zonula occludens-1 ZO-1, cingulin, and junctional adhesion molecule-A JAM-A (Fig. 1B and fig. S2) and AJ formed by vascular endothelial cadherin (VE-cadherin) and β-catenin (Fig. 1C and fig. S3). Claudin-5 was expressed primarily in lymphatic endothelial TJ (fig. S4). Claudin-12 was associated with other cell types in the lamina propria (fig. S2), which probably reflects a function in ion transport rather than in sealing (*10*). Finally, we found that gut ECs were surrounded by enteric glial cells expressing the intermediate filament glial fibrillary acidic protein (GFAP) and by pericytes expressing desmin (Fig. 1D and fig. S5). Thus, gut ECs are organized in a gut-vascular unit and express TJ and AJ proteins.

We then analyzed the expression of plasmalemma vesicle–associated protein-1 (PV1) (*11*), a marker of EC permeability (*12*, *13*). We found that gut blood ECs in the lamina propria (but not in the submucosa) did not express PV1 (Fig. 2A). We then hypothesized that PV1 expression could be modulated upon *Salmonella* challenge, which would reflect the increased vessel permeability. We observed a peak of PV1 up-regulation on blood but not lymphatic vessels in the jejunum and ileum 6 hours after *Salmonella* infection (Fig. 2, A and B). This correlated with *Salmonella* dissemination to the liver and spleen (Fig. 2C) and

[1]Department of Experimental Oncology, European Institute of Oncology, Milan, Italy. [2]The Italian Foundation for Cancer Research (FIRC) Institute of Molecular Oncology (IFOM), Milan, Italy. [3]First Department of Medicine, St. Matteo Hospital, University of Pavia, Pavia, Italy. [4]Unità Operativa Gastroenterologia ed Endoscopia, Fondazione IRCCS Cà Granda, Ospedale Maggiore Policlinico di Milano, and Dipartimento di Fisiopatologia Medico-Chirurgica e dei Trapianti, Università degli Studi di Milano, Milan, Italy. [5]Department of Pathology and Laboratory Medicine, European Institute of Oncology, Milan, Italy. [6]Department of Biosciences, Università degli Studi di Milano, Italy. [7]Department of Genetics, Immunology and Pathology, Uppsala University, Uppsala, Sweden.
***Corresponding author. E-mail: maria.rescigno@ieo.eu**

Editor's Summary

Nlrp6 keeps gut infections in check

Most viruses infect only certain cells of the body. Enteric viruses, such as norovirus and rotavirus, specifically infect the gut. Wang *et al.* now show that the response to such viruses is tissue-specific, too. Antiviral immunity to enteric but not systemic viral infections in mice required Nlrp6, a member of the NOD-like receptor family of proteins that play important roles in host defense. Together with the RNA helicase protein Dhx15, Nlrp6 bound viral RNA and elicited downstream antiviral immune responses necessary for viral clearance. These included the production of type I and type III interferons and the expression of interferon-stimulated genes.

Science, this issue p. 826